Hindawi Publishing Corporation
Mathematical Problems in Engineering
Volume 2013, Article ID 460281, 17 pages
http://dx.doi.org/10.1155/2013/460281

Research Article

On the Discrete-Time Modeling of a DC-to-DC Power Converter and Control Design with Discrete-Time Sliding Modes

Jorge Rivera,[1] Florentino Chavira,[1] and Alexander Loukianov[2]

[1] *Universidad de Guadalajara, Boulevard Marcelino Garcia Barragan 1421, 44430 Guadalajara, JAL, Mexico*
[2] *Cinvestav IPN, Universidad de Guadalajara, Boulevard del Bosque 1145, 45019 Zapopan, JAL, Mexico*

Correspondence should be addressed to Jorge Rivera; jorge.rivera@cucei.udg.mx

Received 1 November 2012; Revised 4 February 2013; Accepted 4 February 2013

Academic Editor: Wei-Chiang Hong

This work presents a novel discrete-time modeling of a boost dc-to-dc power converter by means of the symplectic Euler method. Then, on the basis of this model, a discrete-time sliding mode regulator is designed in order to force the power converter to behave as a dc-to-ac power converter. Simulation and experimental results are carried on, where the great performance of the proposed methodology is verified.

1. Introduction

Switched mode dc-to-dc converters as in [1, 2] are mainly used as constant current sources for LED, LED flashlights, industry lighting, mobile phones, and automotive applications as in [3], among other commercial devices. With respect to dc-to-ac power conversion using the traditional switched dc-to-dc power converter topologies has recently attracted the attention of researchers. So far, various control techniques, either linear or nonlinear, to regulate these converters have been proposed, such as I/O feedback linearization [4], linear designs [5], sliding mode control [6, 7], current-mode-control [8], artificial neural networks [9], fuzzy logic control [10], and passivity-based control [11], among others. Since dc-to-dc converters are absolutely nonlinear systems, for better performance, adopting nonlinear control methods is a good solution.

It is worth mentioning that all of the previously cited works are designed in the continuous-time domain and have been digitally implemented. The recent advancements in digital microprocessor technology have rendered cheaper, simpler, and more flexible digital implementation of control algorithms designed in the continuous-time setting. The main problem is the degradation of the expected performance, due to the fact that the designing of the control law does not take into account the sampled dynamics of the system. This problem motivates the following possible solutions:

(1) the designing of the control law in the continuous-time setting and its implementation by means of zero-order holder;

(2) the exact sampling of the continuous-time system and the designing of the control law in the digital setting;

(3) the use of much simpler discretization methods, such as those due to Euler (explicit or implicit), and the designing of the control law in the digital setting.

The first solution has the drawback of possible poor performance of the resulting sampled controller. For the second solution, the problem of exact sampling of continuous-time systems is not trivial. In fact, in general, a sampled closed representation of the sampled dynamics does not exist; whereas for linear systems, a sampled model in closed form can be easily obtained [12]; for nonlinear systems in general, the sampled data representations are given in the form of infinite series [13]. Hence, in practice, one uses truncated models of desired approximation [7]. The third solution [14] has the disadvantage that the accuracy of the

resulting approximate discrete-time system decreases as the sampling period increases. But, there is an alternative to these approaches that is only valid for dynamical systems modeled by Euler-Lagrange methodology, the use of variational integrators as the symplectic Euler method. The advantages of this method are explained and compared with common Euler (explicit or implicit) methods in [15], and the application in robotics has been satisfactory developed in [16] and electric motors in [17].

On the other hand, the sliding mode control [18] is a popular technique among control engineer practitioners due to the fact that introduces robustness to unknown bounded perturbations that belong to the control subspace; moreover, the residual dynamics under the sliding regime, that is, the sliding mode dynamics, can easily be stabilized with a proper choice of the sliding surface. For an insightful treatment of the sliding mode technique, we refer the reader to the book entitled "Sliding mode control in electro-mechanical systems," [19]. Electrical and electromechanical systems become vulnerable when output tracking signals present small oscillations of finite frequency known as chattering. The chattering problem is harmful because it leads to low control accuracy, high wear of moving mechanical parts, and high heat losses in power circuits. The chattering phenomenon can be caused by the deliberate use of classical sliding mode control technique. This control technique is characterized by a discontinuous control action with an ideal infinite frequency. When fast dynamics are neglected in the mathematical model such phenomenon can appear. Another situation responsible for chattering is due to implementation issues of the sliding mode control signal in digital devices operating with a finite sampling frequency, where the ideal infinite switching frequency of the control signal cannot be fully implemented, [20].

Therefore, in this work one proposes to derive a novel sampled model for the boost converter by means of a variational integrator. For that reason, a Lagrangian formulation for the dc-to-dc boost converter must be first established in order to apply the symplectic Euler method. Then, on the basis of the obtained sampled model a discrete-time sliding mode controller is designed in order to force the dc-to-dc boost converter to behave as a dc-to-ac converter.

The rest of this work is organized as follows: Section 2 describes the discrete Lagrangian mechanics for conservative and nonconservative systems. Section 3 deals with the discrete-time modeling of the boost power converter by means of its Lagrangian formulation. The control algorithm is designed in Section 4 based on a discrete-time sliding mode regulator technique. Section 5 deals with the presentation of simulation and real-time results. Finally, some comments conclude the work.

2. Lagrangian Mechanics and Variational Integrators

In this section, the basic principles of Lagrangian mechanics and discrete Lagrangian mechanics are reviewed from a variational point of view.

2.1. Continuous-Time Lagrangian Mechanics. To define a mechanical system, let Q be a smooth manifold, called the configuration space, and let TQ be its tangent bundle, called the phase space. The Lagrangian is a function $L : TQ \to \Re$ and is commonly defined as the kinetic energy K (usually, the only function of the velocity) minus the potential energy U of the system (usually, the only function of the state variable):

$$L(q, \dot{q}) = K(\dot{q}) - U(q). \tag{1}$$

The functional action is then introduced as the integral of L along a path $q(t)$ for time $t \in [0, T]$:

$$S(q) = \int_0^T L(q, \dot{q})\, dt. \tag{2}$$

With this definition, the main result of Lagrangian dynamics, Hamilton's principle, can be expressed quite simply: this variational principle states that the correct path of motion of a dynamical system is such that its action has a stationary value; that is, the integral along the correct path has the same value as within first-order infinitesimal perturbations. As an integral principle this description encompasses the entire motion of a system between two fixed times (0 and T in our setup). In more ways than one, this principle is very similar to a statement on the geometry of the path $q(t)$: the action can be seen as the analog of a measure of curvature, and the path is such that this curvature is extremized (i.e., minimized or maximized).

In order to determine the path which optimizes the action we take a variation. A variation of the path q is written as δq and can be thought of as an infinitesimal perturbation to the path at each point, with the important property that the perturbation is null at the endpoints of the path. Computing variations of the action induced by variations δq of the path $q(t)$ results in

$$\begin{aligned} \delta S(q) &= \delta \int_0^T L(q(t), \dot{q}(t))\, dt \\ &= \int_0^T \left[\frac{\partial L}{\partial q} \delta q + \frac{\partial L}{\partial \dot{q}} \delta \dot{q} \right] dt \\ &= \int_0^T \left[\frac{\partial L}{\partial q} - \frac{d}{dt}\left(\frac{\partial L}{\partial \dot{q}} \right) \right] \delta q\, dt + \left[\frac{\partial L}{\partial \dot{q}} \delta q \right]_0^T, \end{aligned} \tag{3}$$

where integration by parts is used in the last equality. When the endpoints of $q(t)$ are held fixed with respect to all variations $\delta q(t)$ (i.e., $\delta q(0) = \delta q(T) = 0$), the most right term in the previous equation vanishes. Therefore, the condition of stationary action for arbitrary variations ∂q with fixed endpoints stated in Hamilton's principle directly indicates that the remaining integrand in the previous equation must be zero for all time t, yielding what is known as the Euler-Lagrange equation:

$$\frac{\partial L}{\partial q} - \frac{d}{dt}\left(\frac{\partial L}{\partial \dot{q}} \right) = 0. \tag{4}$$

For a given Lagrangian, this formula will give the equations of motion of the system. Finally to account for nonconservative forces or dissipation F, the least action principle is modified as follows:

$$\delta \int_0^T L\left(q\left(t\right), \dot{q}\left(t\right)\right) dt + \int_0^T F\left(q\left(t\right), \dot{q}\left(t\right)\right) \cdot \delta q dt = 0, \quad (5)$$

this is known as the Lagrange-d'Alembert principle.

2.2. Discrete Mechanics and Variational Integrators. The idea of variational integrators was studied in [21, 22], among others, and a general theory was developed over the subsequent decade (see [23] for a comprehensive survey). The main idea when deriving discrete geometric mechanics is to handle the variational nature of mechanics and to preserve this variational structure in the discrete setting. In fact, very few integrators have a variational nature: the simpler Euler methods as the explicit and the implicit ones are not variational, and both are characterized by demanding small sampling periods in order to perform satisfactorily. Instead of simply approximating the Euler-Lagrange equation to first (or higher) order, one can directly discretize the variational principle behind it. That is, if one designs a discrete equivalent of the Lagrangian, then, a discrete Euler-Lagrange equation can be easily derived from it by paralleling the derivations followed in the continuous case. In essence, good numerical methods will come from discrete analogs to the Euler-Lagrange equation, that is, equations that truly derive from a variational principle.

Suppose that we wish to discretize a mechanical system, whose continuous Lagrangian is $L : TQ \rightarrow \mathfrak{R}$, on the time interval $t \in [0, T]$. First, we partition the time interval by a finite number of points $0 = t_0, \ldots, t_N = T$ where $k, N \in \mathsf{N}$; likewise, the path $q : [0, T] \rightarrow Q$ is replaced by a sequence of configurations $q_0, \ldots, q_N$, where $q_k \approx q(t_k)$. Then the *discrete Lagrangian* is a function $L_d : Q \times Q \rightarrow \mathfrak{R}$ that approximates the Lagrangian L on each time interval $[t_k, t_{k+1}]$, with h being the time interval between two samples $h = t_{k+1} - t_k$ (chosen here to be constant for simplicity), so that

$$L_d\left(q_k, q_{k+1}\right) \approx \int_{t_k}^{t_{k+1}} L\left(q, \dot{q}\right) dt. \quad (6)$$

Now, the right-hand side integral can be approximated through a generalized midpoint quadrature rule; that is, by the length of the interval times the value of the integrand is evaluated somewhere between q_k and q_{k+1} and with $\dot{q}$ replaced by $(q_{k+1} - q_k)/h$:

$$L_d\left(q_k, q_{k+1}, h\right) = hL\left(\left(1-\alpha\right) q_k + \alpha q_{k+1}, \frac{q_{k+1} - q_k}{h}\right), \quad (7)$$

where $\alpha \in [0, 1]$ is parameter that generalizes the quadrature rule. For $\alpha = 1/2$, the quadrature is second-order accurate, while any other value leads to linear accuracy. Also, one can approximate the right-hand side integral through a generalized trapezoidal quadrature rule:

$$\begin{aligned} L_d\left(q_k, q_{k+1}, h\right) &= h\left(1-\alpha\right) L\left(q_k, \frac{q_{k+1} - q_k}{h}\right) \\ &\quad + h\alpha L\left(q_{k+1}, \frac{q_{k+1} - q_k}{h}\right), \end{aligned} \quad (8)$$

where again $\alpha \in [0, 1]$ is parameter that generalizes the quadrature rule and for $\alpha = 1/2$, the quadrature is second-order accurate, meanwhile any other value leads to linear accuracy.

Remark 1. When the integrals are approximated by a generalized midpoint quadrature rule and α is fixed to 0 the variational integrator is known as the symplectic Euler method; when α is fixed to $1/2$ the variational integrator is known as the midpoint Euler method. On the other hand, when the integrals are approximated by the generalized trapezoidal quadrature rule and α is fixed to $1/2$ the variational integrator is known as the Störmer/Verlet method.

Given the discrete Lagrangian, the discrete functional action becomes simply a sum:

$$\begin{aligned} S_d &:= S_d\left(\{q_i\}_{i=0\cdots N}\right) = \sum_{k=0}^{N-1} L_d\left(q_k, q_{k+1}\right) \\ &\approx \int_a^b L\left(q, \dot{q}\right) dt = S\left(q\right). \end{aligned} \quad (9)$$

Taking fixed-endpoint variations of this discrete action S_d, we obtain

$$\begin{aligned} \delta S_d &= \delta \sum_{k=0}^{N-1} L_d\left(q_k, q_{k+1}\right) = \sum_{k=0}^{N-1} D_1 L_d\left(q_k, q_{k+1}\right) \cdot \delta q_k \\ &\quad + \sum_{k=0}^{N-1} D_2 L_d\left(q_k, q_{k+1}\right) \cdot \delta q_{k+1} \\ &= \sum_{k=1}^{N-1} \left[D_2 L_d\left(q_{k-1}, q_k\right) + D_1 L_d\left(q_k, q_{k+1}\right)\right] \cdot \delta q_k \\ &\quad + D_1 L_d\left(q_0, q_1\right) \delta q_0 + D_2 L_d\left(q_{N-1}, q_N\right) \cdot \delta q_N, \end{aligned} \quad (10)$$

where $D_1 L$ (resp., D_2) denotes the partial derivative with respect to the first (resp., second) arguments of L_d. Using the fixed endpoint condition $\delta q_0 = \delta q_N = 0$, one gets

$$\delta S_d = \sum_{k=1}^{N-1} \left[D_1 L_d\left(q_k, q_{k+1}\right) + D_2 L_d\left(q_{k-1}, q_k\right)\right] \cdot \delta q_k. \quad (11)$$

Setting this variation to be equal to 0 and noting that each δq_k is arbitrary, we arrive at the discrete Euler-Lagrange (DEL) equation

$$D_1 L_d\left(q_k, q_{q+1}\right) + D_2 L_d\left(q_{k-1}, q_k\right) = 0. \quad (12)$$

Notice that this condition only involves three consecutive positions. Therefore, for two given successive positions q_k

and q_{k+1}, (12) defines q_{k+2}. Thus, these equations of motion are actually the algorithm for an integrator. And since the DEL equation derives from the extremization of a discrete action, such an algorithm enforces the variational aspect of the motion numerically.

If we take initial conditions (q_0, q_1), then the discrete Euler-Lagrange equations define a recursive rule for calculating the sequence $\{q_k\}_{k=0}^{N}$. Regarded in this way, they define a map $(q_k, q_{k+1}) \rightarrow (q_{k+1}, q_{k+2})$ which we can think of as a one-step integrator for the system defined by the continuous Euler-Lagrange equations.

We are primarily interested in discrete Lagrangian mechanics for deriving integrators. Any integrator which is the discrete Euler-Lagrange equation for some discrete Lagrangian is called a variational integrator. As we have seen previously, variational integrators can be implemented by taking two configurations q_0 and q_1 of the system, which should approximate $q_0 \approx q(t_0)$ and $q_1 \approx q(t_0 + h)$ and then solve the discrete Euler-Lagrange equation (12) for q_2. This process can then be repeated to calculate an entire discrete trajectory. The map $(q_{k-1}, q_k) \rightarrow (q_k, q_{k+1})$ defined by the discrete Euler-Lagrange equations is known as the discrete evolution map.

In mechanics, the initial conditions are typically specified as a position and a velocity or momentum rather than two positions, hence it is beneficial to write (12) in a position-momentum form [24]. Therefore one defines the momentum at time t_k to be

$$p_k := D_2 L_d\left(q_{k-1}, q_k\right) = -D_1 L_d\left(q_k, q_{q+1}\right), \tag{13}$$

where the second equality holds due to (12). The position-momentum form of the variational integrator discussed previously is then given by

$$p_k = -D_1 L_d\left(q_k, q_{k+1}\right), \tag{14}$$

$$p_{k+1} = D_2 L_d\left(q_k, q_{k+1}\right). \tag{15}$$

For (q_k, p_k) known, (14) is an implicit equation whose solution gives q_{k+1}. q_{k+1} is then substituted in (15) in order to find p_{k+1}. This provides an update rule in phase space.

Now we consider nonconservative systems, those with forcing and/or dissipation; in such case, the discrete action can be modified by adding the nonconservative force term and using the discrete Lagrange-d'Alembert principle as in [23]:

$$\begin{aligned}\delta S_d = \delta \sum_{k=0}^{N} L_d\left(q_k, q_{k+1}\right) \\ + \sum_{k=0}^{N} \left[F_d^-\left(q_k, q_{k+1}\right) \cdot \delta q_k + F_d^+\left(q_{k-1}, q_k\right) \cdot \delta q_{k+1}\right] = 0,\end{aligned} \tag{16}$$

where $F_d^-(q_k, q_{k+1})$ and $F_d^+(q_k, q_{k+1})$ are discrete external forces acting, respectively, on the right of q_k and on the left of q_{k+1}. In other words, $F_d^-(q_k, q_{k+1}) \cdot \delta q_k + F_d^+(q_{k-1}, q_k) \cdot \delta q_{k+1}$ can be seen as a two-point quadrature approximation of the continuous forcing term, that is,

$$F_d^-\left(q_k, q_{k+1}\right) \cdot \delta q_k + F_d^+\left(q_{k-1}, q_k\right) \cdot \delta q_{k+1} \approx \int_{t_k}^{k+1} F \cdot \delta q dt. \tag{17}$$

It follows that the forced discrete Euler-Lagrange equation is as follows:

$$\begin{aligned}D_1 L_d\left(q_k, q_{q+1}\right) + D_2 L_d\left(q_{k-1}, q_k\right) \\ + F_d^-\left(q_k, q_{k+1}\right) + F_d^+\left(q_{k-1}, q_k\right) = 0.\end{aligned} \tag{18}$$

The forced discrete Euler-Lagrange equation can be expressed in a convenient, position-momentum form as follows:

$$\begin{aligned}p_k &= -D_1 L_d\left(q_k, q_{k+1}\right) - F_d^-\left(q_k, q_{k+1}\right), \\ p_{k+1} &= D_2 L_d\left(q_k, q_{k+1}\right) + F_d^+\left(q_k, q_{k+1}\right).\end{aligned} \tag{19}$$

This variational treatment of energy decay, despite its simplicity, has also been proven to be superior to the usual time integration schemes that often add numerical viscosity to get stability [24].

3. Discrete-Time Modeling for a Boost Power Converter

In this section, a Lagrangian approach is used for deriving a novel discrete-time model for the boost power converter. The Lagrangian modeling is based on a suitable parametrization, in terms of the switch position parameter, of the EL functions describing each intervening system and subsequent application of the Lagrange formalism.

3.1. Discrete-Time Euler-Lagrange Modeling for a Boost Power Converter. Let us define $\mathsf{T}_u(\dot{q}_L)$ and $\mathsf{V}_u(q_C)$ as the kinetic and potential energies of the circuit, respectively. One can denote by $\mathsf{F}_u(\dot{q})$ the Rayleigh dissipation function of the circuit and by $\mathsf{V}_{u,\mathrm{nc}}(q)$ the nonconservative potential function. These quantities are taken from [25] where they readily are found to be

$$\begin{aligned}\mathsf{T}_u\left(\dot{q}_L\right) = \frac{1}{2} L \dot{q}_L^2, \qquad \mathsf{V}_u\left(q_C\right) = \frac{1}{2C} q_C^2, \\ \mathsf{F}_u\left(\dot{q}\right) = \frac{1}{2} R\left((1-u)\,\dot{q}_L - \dot{q}_C\right)^2, \qquad \mathsf{V}_{u,\mathrm{nc}}\left(q\right) = -\mu^T q,\end{aligned} \tag{20}$$

where q_L and q_C are the circulating charge in the inductor and the electrical charge stored in the output capacitor, respectively, with $q = (q_L, q_C)^T$; moreover, $\dot{q}_L$and $\dot{q}_C$ are the corresponding currents with $\dot{q} = (\dot{q}_L, \dot{q}_C)$, the constant parameters are L as the inductance, C as the capacitance, and R as the resistance. The vector μ is defined as $\mu = (E, 0)^T$, where E is the dc power supply value. Figure 1 shows an electric diagram of a boost power converter circuit.

Now, a nonconservative Lagrangian can be formulated as follows:

$$\mathsf{L}_{\mathrm{nc}}(q,\dot{q}) = \mathsf{L}_c(q,\dot{q}) + \int_0^T \mathsf{F}(\dot{q})\,dt - \mathsf{V}_{\mathrm{nc}}(q), \tag{21}$$

where $\mathsf{L}_c(q,\dot{q})$ is the conservative Lagrangian defined as usual:

$$\mathsf{L}_c(q,\dot{q}) = \mathsf{T}_u(\dot{q}_L) - \mathsf{V}_u(q_C) = \frac{1}{2}L\dot{q}_L^2 - \frac{1}{2C}q_C^2. \tag{22}$$

Following (7) one can obtain the discrete-time version of the conservative Lagrangian as

$$\mathsf{L}_{c,d} = h\frac{1}{2}L\left(\frac{q_{L,k+1}-q_{L,k}}{h}\right)^2 - h\frac{1}{2C}\left((1-\alpha)\,q_{C,k} + \alpha q_{C,k+1}\right)^2. \tag{23}$$

Moreover the discrete external forces $F_d^-(q_k,q_{k+1})$ and $F_d^+(q_k,q_{k+1})$ appearing in (19) are as follows:

$$\begin{aligned} F_d^-(q_k,q_{k+1}) &= h\left(Q_d\left(q_k,q_{k+q}\right) + \mu_d^T\right)(1-\alpha), \\ F_d^+(q_k,q_{k+1}) &= h\left(Q_d\left(q_k,q_{k+q}\right) + \mu_d^T\right)(\alpha), \end{aligned} \tag{24}$$

where $\mu_d = (E,0)^T$ and Q_d are the sampled version of the external generalized forces of control input forces and dissipation forces, respectively. The vector of dissipation forces are obtained as

$$Q = -\frac{\partial \mathsf{F}_u(\dot{q})}{\partial \dot{q}}, \tag{25}$$

where its sampled version is as follows:

$$Q_d = \left(Q_{d,L}\;\; Q_{d,C}\right) = \int_{t_k}^{t_{k+1}} Q\,dt, \tag{26}$$

where again, the right-hand side integral can be approximated through a one-point quadrature, resulting as follows:

$$\begin{aligned} Q_{d,L} &= -R\left((1-u)\left(\frac{q_{L,k+1}-q_{L,k}}{h}\right)\right)(1-u) \\ &\quad + R\left(\frac{q_{C,k+1}-q_{C,k}}{h}\right)(1-u), \\ Q_{d,C} &= R\left((1-u)\left(\frac{q_{L,k+1}-q_{L,k}}{h}\right)\right) - R\left(\frac{q_{C,k+1}-q_{C,k}}{h}\right). \end{aligned} \tag{27}$$

After some algebraic steps and assigning $\alpha = 0$ (i.e., the symplectic Euler method), the updated rule for position shown in (19) yields to

$$P_k = Aq_{k+1} - Aq_k + Bq_k - V, \tag{28}$$

where $P_k = (P_{L,k}, P_{C,k})^T$ and $q_k = (q_{L,k}, q_{C,k})^T$; moreover,

$$A = \begin{pmatrix} \frac{L}{h} + R(1-u)^2 & -R(1-u) \\ -R(1-u) & R \end{pmatrix}, \qquad B = \begin{pmatrix} 0 & 0 \\ 0 & \frac{h}{C} \end{pmatrix},$$
$$V = \begin{pmatrix} hE \\ 0 \end{pmatrix}. \tag{29}$$

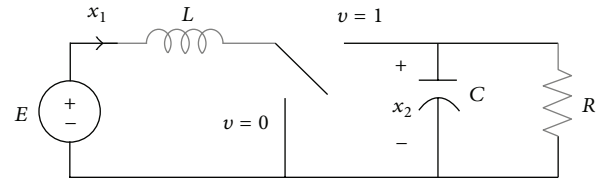

Figure 1: Boost converter circuit.

Then, solving (28) for q_{k+1} results in

$$q_{k+1} = q_k + A^{-1}P_k - A^{-1}Bq_k + A^{-1}V \tag{30}$$

and finally in scalar form:

$$\begin{aligned} q_{L,k+1} &= q_{L,k} - \frac{v_k h^2}{LC}q_{C,k} + \frac{h}{L}P_{L,k} + \frac{h^2 E}{L}, \\ q_{C,k+1} &= q_{C,k} - \frac{\left(L + Rhv_k^2\right)h}{RLC}q_{C,k} + \frac{v_k h}{L}P_{L,k} + \frac{v_k h^2 E}{L}, \end{aligned} \tag{31}$$

where $v_k = 1 - u_k$.

Now, the updated rule for momentum equation shown in (28) yields to

$$\begin{aligned} P_{L,k+1} &= \frac{h}{L}\left(q_{L,k+1} - q_{L,k}\right), \\ P_{C,k+1} &= 0. \end{aligned} \tag{32}$$

Then, by replacing (30) in (32) it yields to

$$P_{L,k+1} = P_{L,k} - \frac{v_k h}{C}q_{C,k} + hE. \tag{33}$$

The variable $q_{L,k}$ can be omitted since it does not enter in the other equations. In the continuous-time model [25] for the boost power converter the first state variable is defined as the derivative of the circulating charge q_L, that is, the input current represented as $x_1 = \dot{q}_L$. The second state variable is defined as the output voltage capacitor and it is represented as $x_2 = q_C/C$ where q_C is the electrical charge stored in the output capacitor. Therefore, one proposes the following novel approximated discrete-time model for the boost power converter:

$$\begin{aligned} \widetilde{x}_{1,k+1} &= \widetilde{x}_{1,k} - \frac{v_k h}{C}\widetilde{x}_{2,k} + hE, \\ \widetilde{x}_{2,k+1} &= \widetilde{x}_{2,k} - \frac{\left(L + Rhv_k^2\right)h}{RLC}\widetilde{x}_{2,k} + \frac{v_k h}{L}\widetilde{x}_{1,k} + \frac{v_k h^2 E}{L}, \\ x_{1,k} &= \frac{\widetilde{x}_{1,k}}{L}, \qquad x_{2,k} = \frac{\widetilde{x}_{2,k}}{C}, \end{aligned} \tag{34}$$

where $\widetilde{x}_{1,k} = P_{L,k}$, $\widetilde{x}_{2,k} = q_{C,k}$, $x_{1,k} \approx x_1(kh)$ is the sampled version of the input current, and $x_{2,k} \approx x_2(kh)$ is the sampled version of the output voltage capacitor.

4. Discrete-Time Control for a Boost Power Converter

There are two options for controlling dc-to-dc power converters, the indirect and direct methods. The first method is characterized by controlling the inductor current where its reference signal is selected such that a desired capacitor voltage is obtained. This has the advantage that the system is minimum phase with respect to the inductor current variable, but the problem consists of guaranteeing the convergence of the output capacitor voltage to its reference signal. In the second method, the output capacitor voltage is directly controlled, where common converter topologies as the boost, buck-boost, and cúk result to be nonminimum phase systems with the main difficulty of stabilizing the unstable inductor current variable [25].

Now, the control problem is formulated. The control problem consists of directly controlling the output capacitor voltage variable $\widetilde{x}_{2,k}$ to track a desired reference signal $\widetilde{x}_{2r,k}(\omega_k)$ and at the same time to stabilize the unstable inductor current variable.

4.1. Sliding Mode Regulator for a Boost Power Converter. Let us define the following tracking error:

$$e_k = \widetilde{x}_{2,k} - \widetilde{x}_{2r,k}\left(\omega_k\right). \tag{35}$$

The reference signal is supposed to be generated by an autonomous exosystem given by

$$\begin{aligned} \omega_{1,k+1} &= \cos(\alpha h)\,\omega_{1,k} - \sin(\alpha h)\,\omega_{2,k}, \\ \omega_{2,k+1} &= \sin(\alpha h)\,\omega_{1,k} + \cos(\alpha h)\,\omega_{2,k0}, \\ \omega_{3,k+1} &= \omega_{3,k}, \end{aligned} \tag{36}$$

with initial conditions $\omega_{1,0} = \omega_{2,0} = a$ and $\omega_{3,0} = b$, with the following output

$$x_{2r,k}\left(\omega_k\right) = \omega_{1,k} + \omega_{3,k}. \tag{37}$$

Then, $x_{2r,k}(\omega_k)$ is a sinusoidal shape signal with amplitude of $\sqrt{2a}$, a frequency equal to α, and a bias value equal to b; moreover, $\omega_k = (\omega_{1,k}, \omega_{2,k}, \omega_{3,k})^T$. Finally one determines that $\widetilde{x}_{2r,k}(\omega_k) = \widetilde{\pi}_{2,k}(\omega_k) = C\pi_{2,k}(\omega_k)$.

We define the steady state error as

$$z_k = \left(z_{1,k}, z_{2,k}\right)^T = \widetilde{x}_k - \widetilde{\pi}_k\left(\omega_k\right), \tag{38}$$

where $\widetilde{x}_k = (\widetilde{x}_{1,k} \quad \widetilde{x}_{2,k})^T$ and $\widetilde{\pi}_k(\omega_k) = (\widetilde{\pi}_{1,k} \quad \widetilde{\pi}_{2,k})^T$ with $\widetilde{\pi}_{1,k} = L\pi_{1,k}$ and $\widetilde{\pi}_{2,k} = C\pi_{2,k}$. Then, the dynamic equation for (38) can be obtained by taking one step ahead:

$$\begin{aligned} z_{1,k+1} &= \widetilde{x}_{1,k} - \frac{v_k h}{C}\widetilde{x}_{2,k} + hE - \widetilde{\pi}_{1,k+1}\left(\omega_k\right), \\ z_{2,k+1} &= \widetilde{x}_{2,k} - \frac{\left(L + Rhv_k^2\right)h}{RLC}\widetilde{x}_{2,k} + \frac{v_k h}{L}\widetilde{x}_{1,k}, \\ &\quad + \frac{v_k h^2 E}{L} - \widetilde{\pi}_{2,k+1}\left(\omega_k\right). \end{aligned} \tag{39}$$

Proposition 2. *Consider the sliding mode function as*

$$s_k = z_{2,k} + c_1 z_{1,k}, \tag{40}$$

and the sliding mode controller:

$$v_k = \begin{cases} v_{eq,k} & \text{if } 0 < v_{eq,k} < 1, \\ \dfrac{1}{2} - \dfrac{1}{2}\dfrac{v_{eq,k}}{\left|v_{eq,k}\right|} & \text{if } 0 > v_{eq,k} > 1, \end{cases} \tag{41}$$

where $v_{eq,k}$ is the equivalent control calculated as usual from $s_{k+1} = 0$ and the design parameter c_1 is chosen such that $a_{11} - a_{12}c_1 = \lambda_1$, with $|\lambda_1| < 1$ and

$$a_{1,j} = \left.\frac{\partial f_{1,k}}{\partial \widetilde{x}_{j,k}}\right|_{(b^2L/(RE),bC)}, \tag{42}$$

with $j = 1, 2$; moreover, $f_{1,k}$ is the right hand of the first equation in (39)*; then, the posed control problem is solved.*

Proof. Condition $s_{k+1} = 0$ results as follows:

$$\begin{aligned} s_{k+1} &= \widetilde{x}_{2,k} - \frac{\left(L + Rhv_k^2\right)h}{RLC}\widetilde{x}_{2,k} \\ &\quad + \frac{v_k h}{L}\widetilde{x}_{1,k} + \frac{v_k h^2 E}{L} - \widetilde{\pi}_{2,k+1}\left(\omega_k\right) \\ &\quad + c_1\left(\widetilde{x}_{1,k} - \frac{v_k h}{C}\widetilde{x}_{2,k} + hE - \widetilde{\pi}_{1,k+1}\left(\omega_k\right)\right) = 0. \end{aligned} \tag{43}$$

After making some simplifications one obtains

$$S_{k+1} = a_k v_{\mathrm{eq},k}^2 + b_k v_{\mathrm{eq},k} + c_k = 0, \tag{44}$$

where

$$\begin{aligned} a_k &= -\frac{h^2}{LC}\widetilde{x}_{2,k}, \\ b_k &= \frac{h}{L}\widetilde{x}_{1,k} + \frac{h^2 E}{L} + c_1\frac{h}{C}\widetilde{x}_{2,k}, \\ c_k &= \left(1 - \frac{h}{RC}\right)\widetilde{x}_{2,k} - \widetilde{\pi}_{2,k+1} + c_1\left(\widetilde{x}_{1,k} + hE - \widetilde{\pi}_{1,k+1}\right). \end{aligned} \tag{45}$$

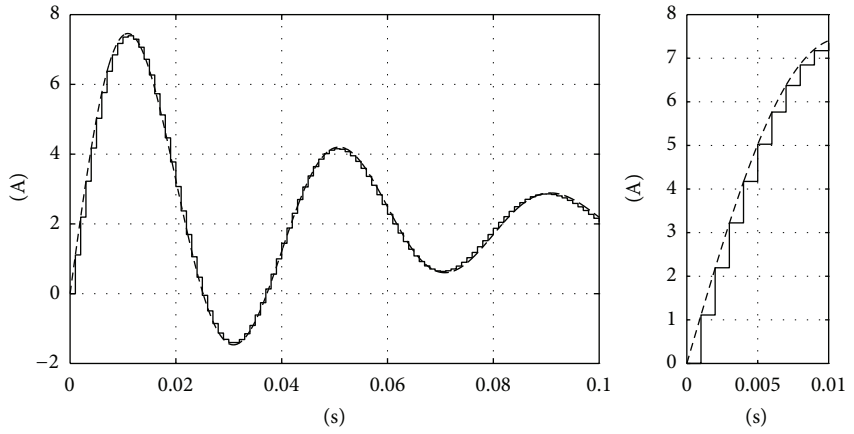

Figure 2: Open-loop current comparison, continuous-time model (dashed line), discrete-time model (solid line).

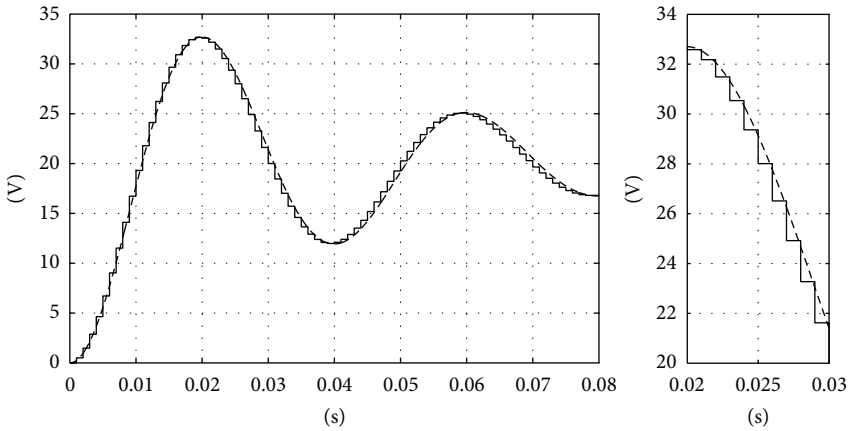

Figure 3: Open-loop voltage comparison, continuous-time model (dashed line), discrete-time model (solid line).

Equation (44) has been dealt in the work presented by [26], where the following equivalent control solution has been proposed:

$$v_{\mathrm{eq},k} = \begin{cases} -\dfrac{b_k}{2a_k} \pm \dfrac{\sqrt{\Delta_k}}{2a_k} & \text{if } a_k > 0,\ \Delta_k \geq 0, \\ -\dfrac{b_k}{2a_k} & \text{if } a_k > 0,\ \Delta_k < 0, \\ -\dfrac{c_k}{b_k} & \text{if } a_k \leq 0, \end{cases} \tag{46}$$

where $\Delta_k = b_k^2 - 4a_k c_k$. With this equivalent control, the sliding function is zeroed in one or more steps or tends asymptotically to zero. When $0 > v_{\mathrm{eq},k} > 1$, the control action is saturated (41). In this case, for analysis purposes, the saturated control can be modified as follows:

$$v_k = v_0 \frac{v_{\mathrm{eq},k}}{\left|v_{\mathrm{eq},k}\right|}, \quad \text{for } \left|v_{\mathrm{eq},k}\right| > v_0, \tag{47}$$

with $v_0 = 1/2$; moreover, after some algebraic steps, the sliding function dynamics (44) can be represented in the following form:

$$S_{k+1} = v_k + \frac{b_k}{2a_k} \mp \frac{\sqrt{\Delta_k}}{2a_k}. \tag{48}$$

In order to reveal the structure of the sliding function dynamics, let us represent it as follows:

$$S_{k+1} = S_k + v_k + \frac{b_k}{2a_k} \mp \frac{\sqrt{\Delta_k}}{2a_k} - z_{2,k} - c_1 z_{1,k}, \tag{49}$$

and the equivalent control in the case of $\Delta_k \geq 0$ is rewritten as follows:

$$v_{\mathrm{eq},k} = -S_k - \frac{b_k}{2a_k} \pm \frac{\sqrt{\Delta_k}}{2a_k} + z_{2,k} + c_1 z_{1,k}. \tag{50}$$

Now suppose that the control can vary within the fictitious bound of v_0, therefore the available control resources are such that

$$\left| \frac{b_k}{2a_k} \mp \frac{\sqrt{\Delta_k}}{2a_k} + z_{2,k} + c_1 z_{1,k} \right| < v_0. \tag{51}$$

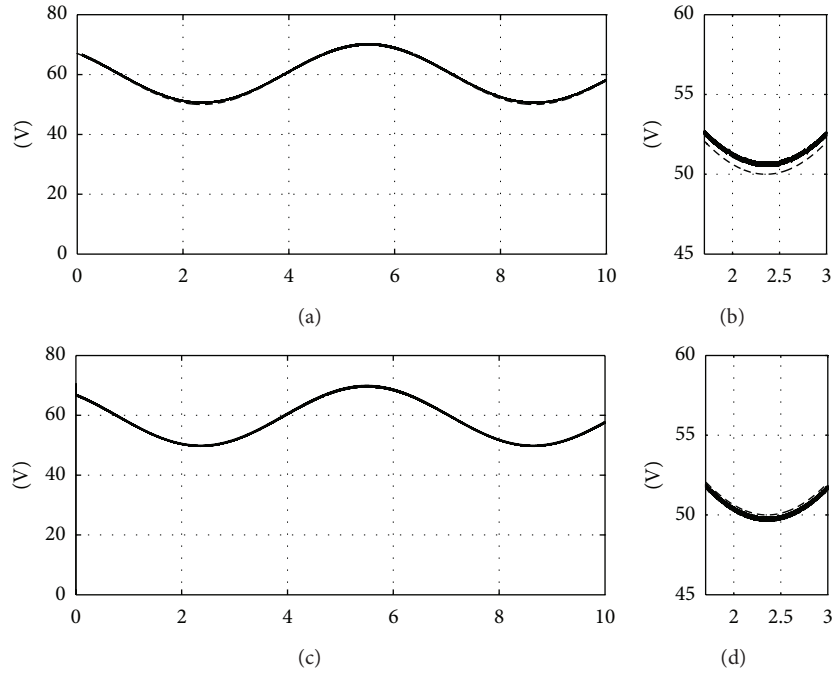

FIGURE 4: Comparison of discrete-time controllers with a sample time of 10 μs. Output capacitor voltage (continuous line), reference signal (dashed line). (a) Output capacitor voltage obtained with sampled controller. (c) Output capacitor voltage obtained with proposed controller. (b) and (d) are zoom views of same variables on the left.

Substituting (50) in (47), and (47) in (49) yields to

$$\begin{aligned} S_{k+1} &= \left(S_k + \frac{b_k}{2a_k} \mp \frac{\sqrt{\Delta_k}}{2a_k} - z_{2,k} - c_1 z_{1,k} \right) \\ &\times \left(1 - \frac{v_0}{\left| -S_k - b_k/2a_k \pm \sqrt{\Delta_k}/2a_k + z_{2,k} + c_1 z_{1,k} \right|} \right), \end{aligned} \tag{52}$$

and by taking the absolute values

$$\begin{aligned} \left| S_{k+1} \right| &= \left| S_k + \frac{b_k}{2a_k} \mp \frac{\sqrt{\Delta_k}}{2a_k} - z_{2,k} - c_1 z_{1,k} \right| \\ &\times \left(1 - \frac{v_0}{\left| -S_k - b_k/2a_k \pm \sqrt{\Delta_k}/2a_k + z_{2,k} + c_1 z_{1,k} \right|} \right) \\ &= \left| S_k + \frac{b_k}{2a_k} \mp \frac{\sqrt{\Delta_k}}{2a_k} - z_{2,k} - c_1 z_{1,k} \right| - v_0. \end{aligned} \tag{53}$$

At this point, one proposes the following candidate Lyapunov function:

$$V_k = \left| S_k \right|, \tag{54}$$

where the increment of the Lyapunov function results as follows:

$$\begin{aligned} \Delta V &= \left| S_{k+1} \right| - \left| S_k \right| \\ &= \left| S_k + \frac{b_k}{2a_k} \mp \frac{\sqrt{\Delta_k}}{2a_k} - z_{2,k} - c_1 z_{1,k} \right| - v_0 - \left| S_k \right| \\ &\leq \left| S_k \right| + \left| \frac{b_k}{2a_k} \mp \frac{\sqrt{\Delta_k}}{2a_k} - z_{2,k} - c_1 z_{1,k} \right| - v_0 - \left| S_k \right|, \end{aligned} \tag{55}$$

and by using condition (51), the increment of the Lyapunov function reduces to $\Delta V < 0$. Therefore, the sliding function (40) and the equivalent control (46) are decreasing monotonically, and after a finite number of steps, $0 < v_{\mathrm{eq},k} < 1$ is achieved. Discrete-time sliding mode will take place from the next sampling point onwards.

Remark 3. When $v_{\mathrm{eq},k} = -b_k/2a_k$ or $v_{\mathrm{eq},k} = -c_k/b_k$ is chosen in (46), a similar Lyapunov analysis can be carried on, where the sliding function (40) can be demonstrated to decrease monotonically.

After the sliding mode occurs, one has $z_{2,k} = -c_1 z_{1,k}$ (see (40)), and considering only the linear part of the first equation of (39) along with (46) as in [19], then, the motion of the linearized closed-loop system (sliding mode motion) will be governed by

$$z_{1,k+1} = \left(a_{11} - a_{12} c_1 \right) z_{1,k} + \phi_{1,s,k} \tag{56}$$

with $\phi_{1,s,k}$ as a function of higher order terms that vanish at the origin with their first derivative; then, one can assign a

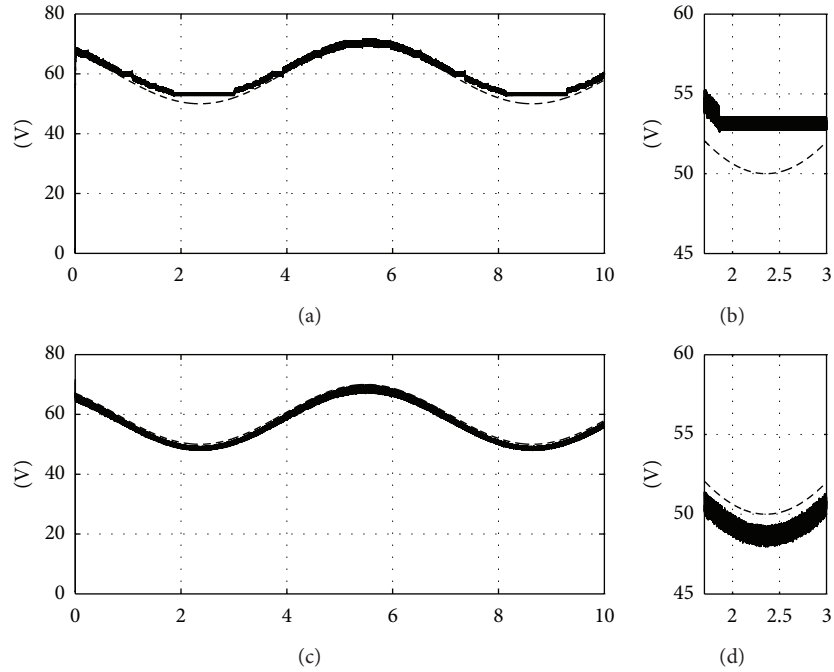

FIGURE 5: Comparison of discrete-time controllers with a sample time of 50 μs. Output capacitor voltage (continuous line), reference signal (dashed line). (a) Output capacitor voltage obtained with sampled controller. (c) Output capacitor voltage obtained with proposed controller. (b) and (d) are zoom views of same variables on the left.

desired eigenvalue and solve for c_1, that is, $a_{11} - a_{12}c_1 = \lambda_1$, with $|\lambda_1| < 1$. With this choice it is easy to realize that the linear approximation of $z_{1,k}$ in the sliding regime (56) is asymptotically stable, and under the property of center manifold, one has a locally attractive manifold on (38), that is, $z_{1,k} \to 0 \Rightarrow \widetilde{x}_{1,k} = \widetilde{x}_{1r,k}$ and $z_{2,k} \to 0 \Rightarrow \widetilde{x}_{2,k} = \widetilde{x}_{2r,k}$ as $k \to \infty$. □

Remark 4. Due to the complexity of the equivalent control (46), the sliding mode dynamics (56) must be determined for the three conditions presented in (46), where the design parameter c_1 must stabilize the sliding mode dynamics for all cases.

4.2. Reference Signal Calculation for the Inductor Current. The smooth mappings $\widetilde{\pi}_{1,k}(\omega_k) : W_0 \to \mathfrak{R}$ and $\widetilde{\pi}_{2,k}(\omega_k) : W_0 \to \mathfrak{R}$ (where W_0 is an open neighborhood of $\omega_k = 0$), with $\widetilde{\pi}_{1,0}(0) = 0$ and $\widetilde{\pi}_{2,0}(0) = 0$, are such that the pair $(\widetilde{\pi}_{1,k}(\omega_k),\ \widetilde{\pi}_{2,k}(\omega_k))$ is the unique solution to the following difference equations:

$$\widetilde{\pi}_{1,k+1}(\omega_k) = \widetilde{\pi}_{1,k}(\omega_k) - \frac{c_k h}{C}\widetilde{\pi}_{2,k}(\omega_k) + hE, \tag{57}$$

$$\begin{aligned}\widetilde{\pi}_{2,k+1}(\omega_k) = \widetilde{\pi}_{2,k}(\omega_k) &- \frac{\left(L + Rhc_k^2\right)h}{RLC}\widetilde{\pi}_{2,k}(\omega_k) \\ &+ \frac{c_k h}{L}\widetilde{\pi}_{1,k}(\omega_k) + \frac{c_k h^2 E}{L},\end{aligned} \tag{58}$$

$$0 = \widetilde{\pi}_{2,k}(\omega_k) - \widetilde{x}_{2k}(\omega_k). \tag{59}$$

From (37) and (59) one can determine $\widetilde{\pi}_{2,k}(\omega_k) = C(\omega_{1,k} + \omega_{3,k})$. Then, one can calculate c_k from (57) as follows:

$$c_k = C\frac{\widetilde{\pi}_{1,k}(\omega_k) + hE - \widetilde{\pi}_{1,k+1}(\omega_k)}{h\widetilde{\pi}_{2,k}(\omega_k)}, \tag{60}$$

and substituting it in (58) yields to

$$\begin{aligned}\widetilde{\pi}_{2,k+1}(\omega_k) = \left(1 - \frac{h}{RC}\right)\widetilde{\pi}_{2,k} &- \frac{C}{L}\frac{\left(\widetilde{\pi}_{1,k+1} - \widetilde{\pi}_{1,k} - hE\right)^2}{\widetilde{\pi}_{2,k}} \\ &- \frac{C}{L}\frac{\left(\widetilde{\pi}_{1,k} + hE\right)\left(\widetilde{\pi}_{1,k+1} - \widetilde{\pi}_{1,k} - hE\right)}{\widetilde{\pi}_{2,k}}.\end{aligned} \tag{61}$$

The finding of a solution to this difference equation results in a difficult task that can be solved by proposing an approximated solution as in [27]. Thus, one proposes the following polynomial as an approximated solution for $\widetilde{\pi}_{1,k}(\omega_k)$:

$$\begin{aligned}\widetilde{\pi}_{1,k}(\omega_k) = a_0 &+ a_1\omega_{1,k}^3 + a_2\omega_{1,k}^2 + a_3\omega_{2,k}\omega_{1,k}^2 \\ &+ a_4\omega_{3,k}\omega_{1,k}^2 + a_5\omega_{1,k}\omega_{2,k}^2 + a_6\omega_{1,k}\omega_{2,k} \\ &+ a_7\omega_{3,k}\omega_{1,k}\omega_{2,k} + a_8\omega_{1,k} + a_9\omega_{3,k}\omega_{1,k} \\ &+ a_{10}\omega_{3,k}^2\omega_{1,k} + a_{11}\omega_{2,k}^3 + a_{12}\omega_{2,k}^2 \\ &+ a_{13}\omega_{3,k}\omega_{2,k}^2 + a_{14}\omega_{2,k} + a_{15}\omega_{3,k}\omega_{2,k} \\ &+ a_{16}\omega_{3,k}^2\omega_{2,k} + a_{17}\omega_{3,k} + a_{18}\omega_{3,k}^2 \\ &+ a_{19}\omega_{3,k}^3 + \mathrm{O}^4\left(\|\omega_k\|_1\right).\end{aligned} \tag{62}$$

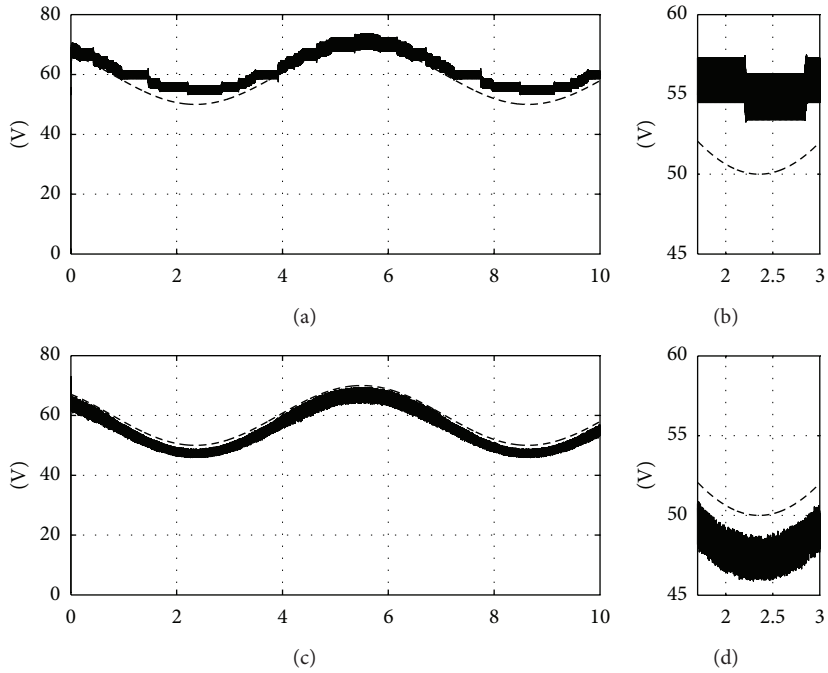

Figure 6: Comparison of discrete-time controllers with a sample time of 100 μs. Output capacitor voltage (continuous line), reference signal (dashed line). (a) Output capacitor voltage obtained with sampled controller. (c) Output capacitor voltage obtained with proposed controller. (b) and (d) are zoom views of same variables on the left.

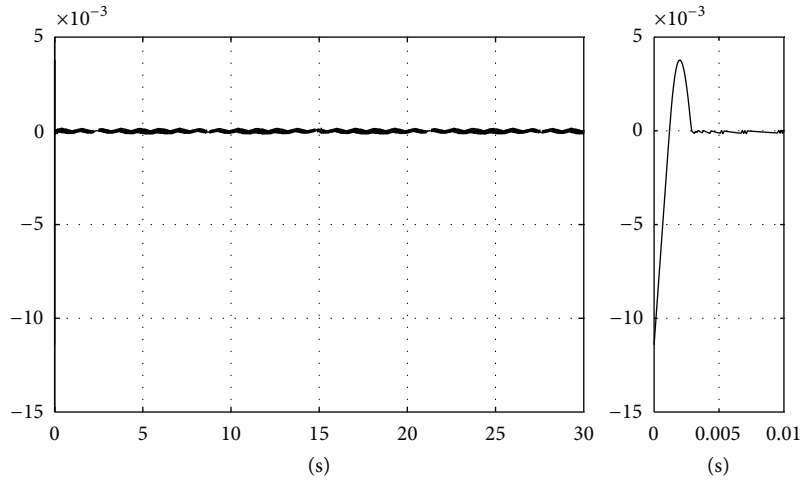

Figure 7: Sliding function with $\alpha = 1$ rad/s.

Multiplying (61) by $\tilde{\pi}_{2,k}(\omega_k)$ and then substituting (62) in the resulting equation, one can find the values $a_i\,(i = 0, \ldots, 19)$ if the coefficients of the same monomials appearing in both sides of such equation are equalized. In that case, the unique coefficients with values different from zero are

$$a_2 = -\frac{L\cos(\alpha h)\left(-\cos(\alpha h)\,h - RC + RC\cos(\alpha h)\right)}{hER},$$

$$a_6 = -\frac{L\sin(\alpha h)\left(-2\cos(\alpha h)\,h - RC + 2RC\cos(\alpha h)\right)}{hER},$$

$$a_9 = -\frac{L\left(RC\cos(\alpha h) - RC - 2\cos(\alpha h)\,h\right)}{hER},$$

$$a_{12} = \frac{(RC - h)\,L\left(-1 + \cos^2(\alpha h)\right)}{hER},$$

$$a_{15} = \frac{(RC - 2h)\,L\sin(\alpha h)}{hER}, \qquad a_{18} = \frac{L}{RE}. \tag{63}$$

Note that the bias value for $\tilde{\pi}_{1,k}(\omega_k)$ is the monomial with a_{18} as a coefficient, that is, $b^2L/(RE)$. This fact was used when linearizing the sliding mode dynamics.

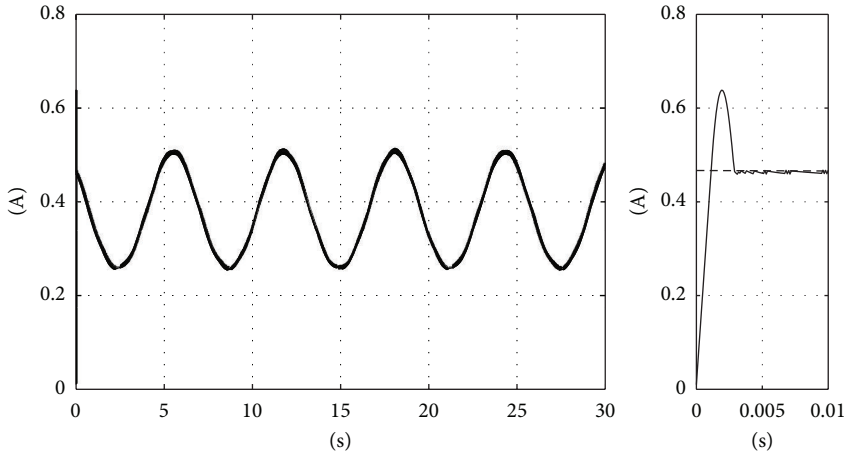

Figure 8: Inductor current tracking with $\alpha = 1$ rad/s, reference signal (dashed line), real signal (solid line).

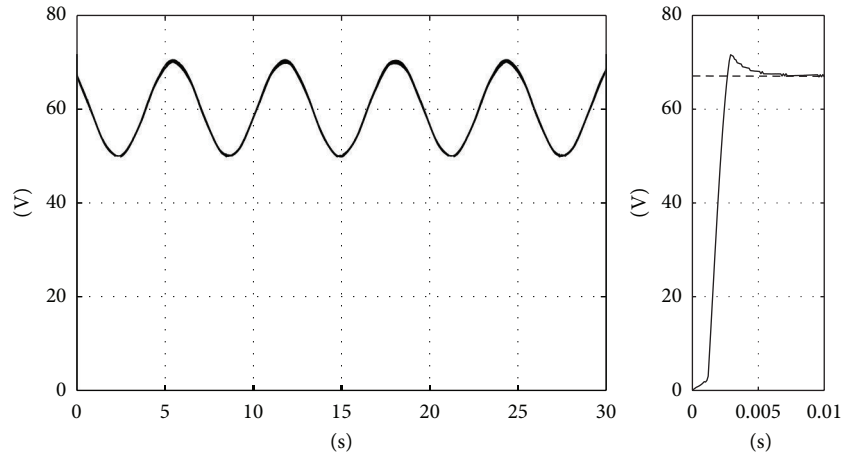

Figure 9: Output tracking of the voltage capacitor with $\alpha = 1$ rad/s, reference signal (dashed line), real signal (solid line).

5. Simulations and Experimental Results

5.1. Open-Loop Simulations. Open-loop simulations were carried out in order to verify the performance of the obtained discrete-time model. The following two figures show the comparison of the continuous-time model of the boost power converter simulated with a sampling time of 0.0001 s and the discrete-time model with a sampling time of 0.001 s. The switch input value was set to $u = 0$. Figure 2 shows the performance of the inductor current, and Figure 3 shows the performance of the output capacitor voltage. In both figures can be appreciated that the discrete-time model it can accurately track the corresponding continuous-time signals.

5.2. Comparison of Two Control Schemes. The designed controller in [28] (see the appendix) is discretized by means of the explicit Euler method and compared with the controller here designed. It is worth mentioning that the discretization of continuous-time controllers via this method is a common practice among control engineer practitioners. Figure 4 shows the performance of the output capacitor voltage with a sample time of 10 μs. In this figure one observes that both controllers have a good tracking performance. Figure 5 shows the simulation with a sample time of 50 μs. In this figure one can observe that the proposed controller still performs well (Figure 5(b)); meanwhile, the sampled controller (Figure 5(a)) shows a difficulty for tracking the reference signal at lower peaks.

Finally, Figure 6 shows simulation results where the sample time is incremented to 100 μs. Here, one can appreciate the difference between the sampling of continuous-time controllers and the discrete-time control law design based on a good sampled model. There is a slight deviation in the output voltage capacitor for the proposed controller as can be seen in Figure 6(c), but, with the sampled controller, the output voltage capacitor signal is distorted (see Figure 6(a)). This is the intention of this simulation exercise, to show the degradation of the discretized controller with larger sampling periods and at the same time to show that the proposed controller can still perform better even with the larger

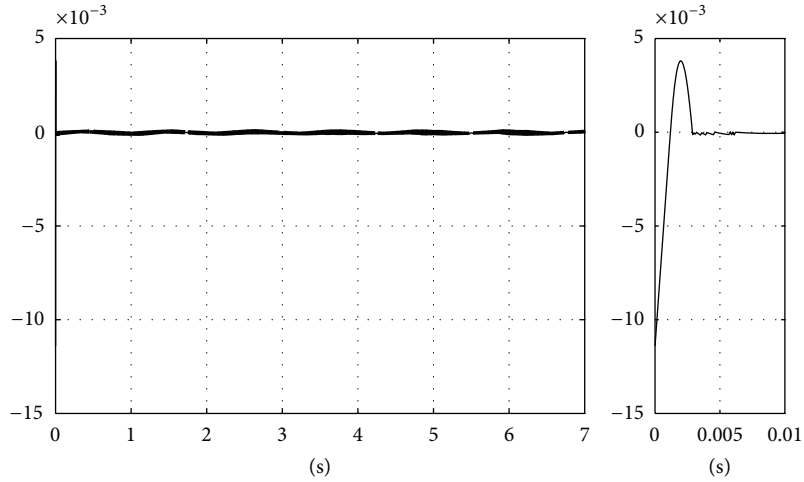

Figure 10: Sliding function with $\alpha = 5$ rad/s.

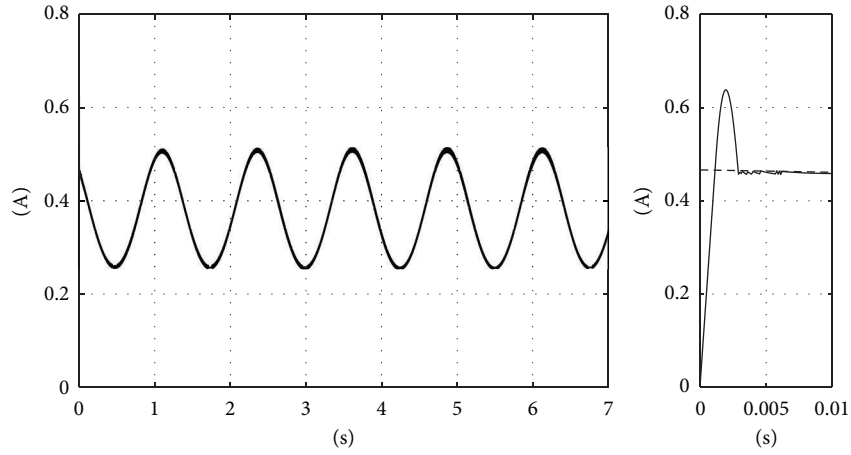

Figure 11: Inductor current tracking with $\alpha = 5$ rad/s, reference signal (dashed line), real signal (solid line).

sampling periods. It is worth mentioning that these discrete-time control laws were simulated with the continuous-time plant model.

5.3. Simulations of the Proposed Control Algorithm. Closed-loop simulations were carried out in order to verify the performance of the proposed controller. The initial conditions for the exosystem (36) are set to $a = 7.071$, $b = 60$ in order to generate a sinusoidal shape signal with amplitude value of 10 and a bias value of 60. The parameters of the boost converter are $L = 0.098\,\text{H}$, $C = 10\,\mu\text{F}$, $R = 241\,\Omega$, and $E = 40\,\text{V}$. The design parameter c_1 in the sliding function (40) is fixed to 1 by means of a trial and error method. In the following, simulation results for the tracking of a sinusoidal signal with frequency of $\alpha = 1$ rad/s will be shown. Figure 7 shows the sliding function where the finite-time convergence can be appreciated.

Figure 8 shows the minimum phase behavior of the inductor current that is commonly known to be a nonminimum phase variable.

The output tracking result of the voltage capacitor can be appreciated in Figure 9.

Now, simulation results for the tracking of a sinusoidal signal with a frequency value of $\alpha = 5$ rad/s will be shown. Figure 10 shows the sliding function where once again the finite-time convergence can be appreciated. Figures 11 and 12 show the good tracking performance of the inductor current and the voltage capacitor, respectively.

5.4. Real-Time Experimentation. The experimental setup is shown in Figure 13. Here, the VARIAC is a three-phase variable transformer fed from a three-phase voltage source. By rotating the knob of the VARIAC, the amplitude of the three-phase voltage source is regulated. These voltages are fed to the power module (Semikron) that incorporates a three-phase rectifier and a single switching transistor that is connected to the boost power converter elements; in that way, a regulated dc input voltage is available for the boost power converter. The control algorithm and PWM generation are programmed in Simulink and implemented with a DSP board

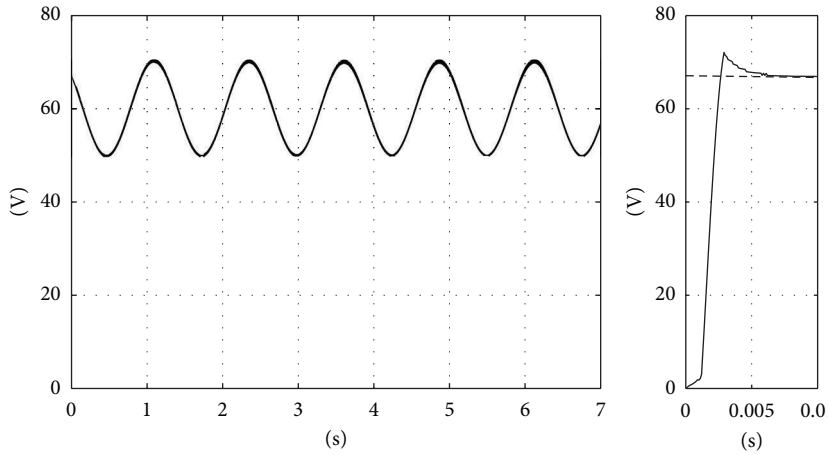

Figure 12: Output tracking of the voltage capacitor with $\alpha = 5$ rad/s, reference signal (dashed line), real signal (solid line).

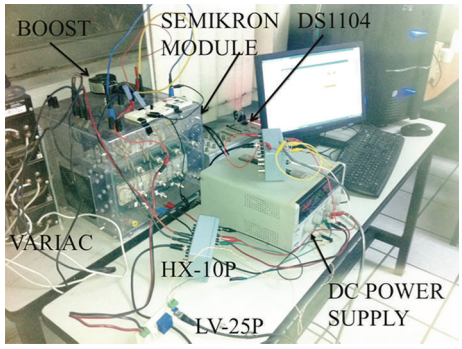

Figure 13: Experimental setup.

(dSPACE 1104). This board comes along with a library that easily incorporates with Simulink.

Analog-to-digital converters included in the DSP board acquire the signals from the inductor current and capacitor voltage. Once the DSP executes the control algorithm in each sampling step, it generates one digital signal for switching the insulated-gate bipolar transistor (IGBT). This digital signal is TTL level and it is converted to a CMOS level of 15 V. This voltage level is the required one for switching on the IGBT. A block diagram of this setup is shown in Figure 14.

The power converter has the same parameter values of the digitally simulated boost circuit in Section 5.2. The inductor current and the output voltage capacitor are measured by means of hall-type sensors, as the HX 10-P and LV 25-P, respectively; both are manufactured by LEM. A first-order Butterworth low-pass filter having an 50 rad/s edge frequency was used for filtering the inductor current in order to attenuate the measurement noise. The sampling period has been fixed at $h = 70\,\mu$s. The dc input voltage E was open loop (the switch position ν_k was set to 1) calibrated to a value of 20 V; then, the boost power converter was closed loop in order that the output voltage capacitor is forced to track a sinusoidal signal with an amplitude of 10 V and bias of 40 V. The real-time results for a frequency value of 1 rad/s are shown in Figures 15 and 16 and for a value of 5 rad/s are shown in Figures 17 and 18. In general, a good output tracking performance in both cases can be appreciated. The tracking of the inductor current shows in both cases big peak values of short duration that are admissible; moreover the first-order filter introduces the appreciated delay.

Remark 5. The tracking of the inductor is not so accurate due to the effect of the PWM switching which is correct since the system is not regulating the inductor current but the capacitor voltage.

In order to better evaluate the control performance, we consider the precision error P_e and the chattering effect C_h. The former is defined as the relative error of the output variable and it is calculated as the difference between the reference value and the average steady-state control output, divided by the reference value

$$P_e = \frac{|S_r - V_{\text{mc}}|}{S_r} \times 100, \tag{64}$$

where S_r is the imposed reference and V_{mc} is the average of the output controlled variable in steady state. The amplitude of the signal characterizes the latter, and it is given by the difference between the amplitude of the output variable and the average in steady state of the reference signal and divided by the latter signal

$$C_h = \frac{|A_{\text{mc}} - V_{\text{mc}}|}{V_{\text{mc}}} \times 100, \tag{65}$$

where A_{mc} is the maximum amplitude of the deviations of controlled signals with respect to its average value V_{mc}. Table 1 summarizes the evaluation parameters for the two frequencies. One can observe that the proposed controller in closed loop yields to small percentiles in precision error and in chattering as well.

Remark 6. The chattering problem can be significantly reduced with the incorporation of soft computing techniques. In particular, sliding mode control when combined with artificial neural networks can be useful to estimate the equivalent

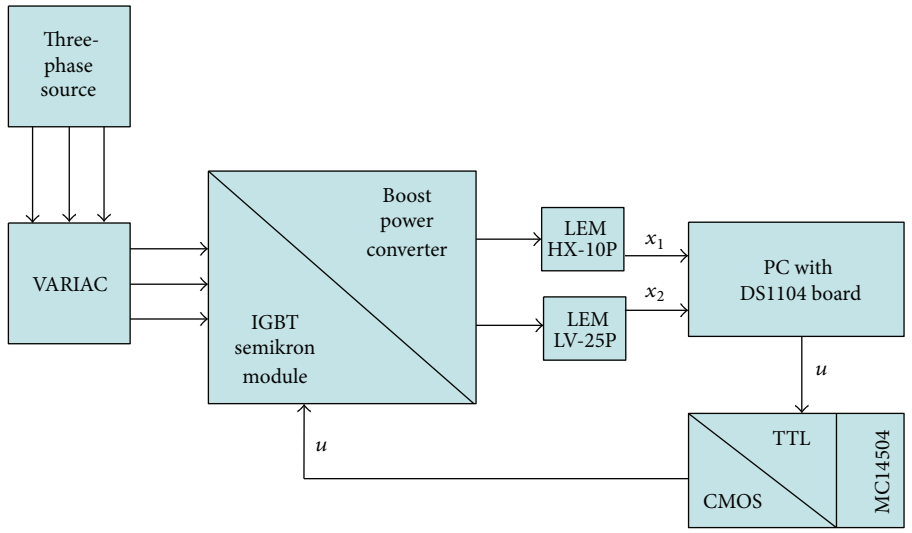

Figure 14: Block diagram of the experimental setup.

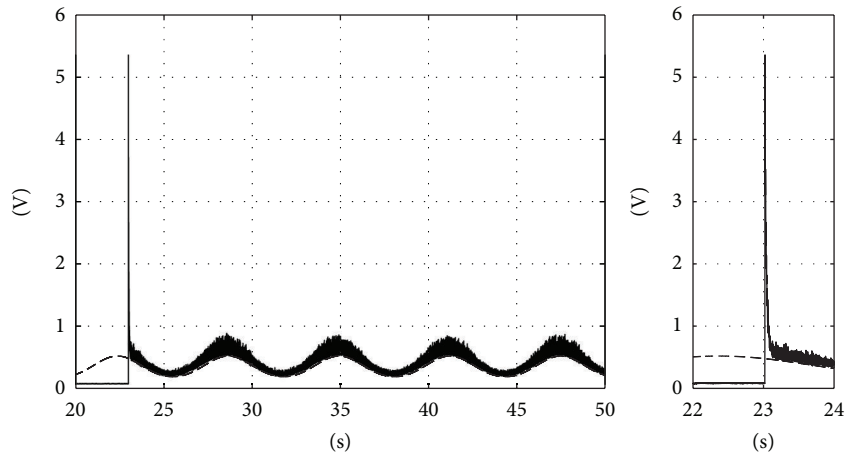

Figure 15: Inductor current tracking with $\alpha = 1$ rad/s, reference signal (dashed line), real-time signal (solid line).

Table 1

Frequency	P_e	C_h
1 rad/s	0.5%	0.67%
5 rad/s	0.5%	0.54%

control and the magnitude of the switching control component using the conventional gradient learning algorithm. On the other hand, instead of using the well-defined sliding mode control functions, the control action can be derived from a fuzzy logic-based control table, compounded by fuzzy membership functions. In such a way, the convergence on the switching manifold and overshooting is softened, alleviating in this way the chattering problem. More directions can be found in [29].

6. Conclusions

A discrete-time sliding mode control scheme has been designed for the dc-to-ac boost power conversion problem. The contributions of this work are the following.

(i) A novel discrete-time model for the boost power converter circuit was obtained by means of a variational integrator scheme.

(ii) The discrete-time-sliding-mode-based controller can stabilize the nonminimum phase system with a proper choice of a sliding surface, resulting in the output tracking of the capacitor voltage and the stabilization of the inductor current.

(iii) The reference signal for the inductor current was proposed as a polynomial of order 3 that solves with a good accuracy the corresponding solution of the reference difference equation.

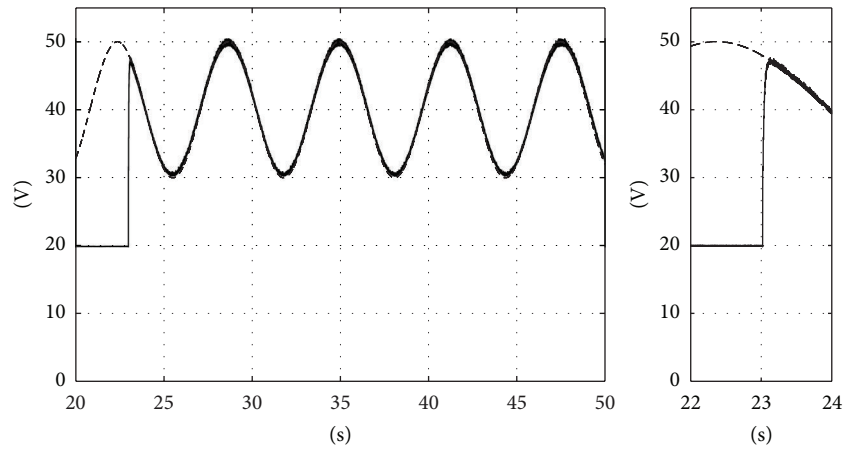

Figure 16: Output tracking of the voltage capacitor with $\alpha = 1$ rad/s, reference signal (dashed line), real-time signal (solid line).

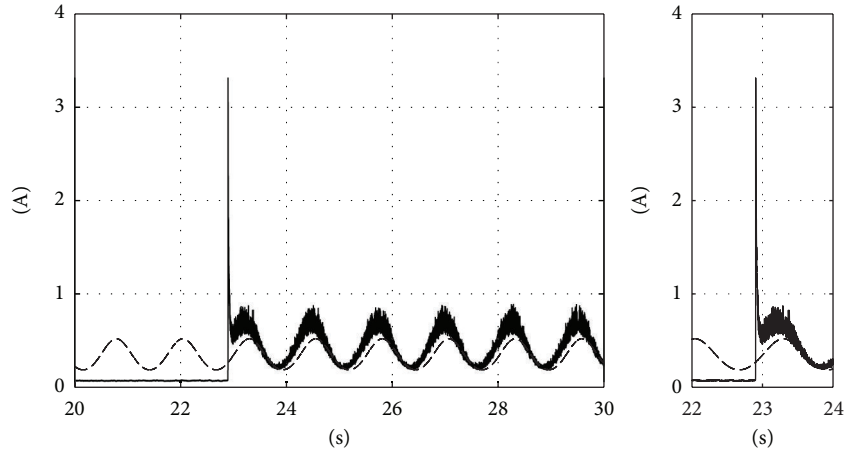

Figure 17: Inductor current tracking with $\alpha = 5$ rad/s, reference signal (dashed line), real-time signal (solid line).

Moreover, simulation and experimental results validate the good performance of the proposed dc-to-ac boost power conversion scheme. Some interesting issues, such as the robustness of the controller with respect to parameter variations, determination of the sampling period, are currently under study.

Appendix

Sampling of a Continuous-Time Controller

Here, we briefly review the control design for a boost converter circuit in the continuous-time setting as presented in [28]. The controller is derived considering that the control problem consists of forcing the output capacitor $y = x_2$ to track a reference signal $x_{2,r}$. The reference signal is supposed to be generated by an autonomous exosystem given by

$$\begin{aligned} \dot{w}_1 &= -\alpha w_2, \\ \dot{w}_2 &= \alpha w_1, \\ \dot{w}_3 &= 0, \end{aligned} \tag{A.1}$$

with initial conditions $w_1(0) = w_2(0) = a$ and $w_3(0) = b$ and with the following output

$$x_{2,r} = w_1 + w_3, \tag{A.2}$$

where w_1 is a sinusoidal shape signal with an amplitude of $\sqrt{2}a$ and a frequency equal to α, w_3 provides a bias value equal to b; moreover, $w = (w_1, w_2, w_3)^T$. The steady state error is defined as follows:

$$z = x - \pi(w) = (z_1, z_2)^T, \tag{A.3}$$

where $x = (x_1, x_2)^T$ and $\pi(w) = (\pi_1(w), \pi_2(w))^T$. The steady state for x_2 is selected as $\pi_2(w) = w_1 + w_3$ and for x_1 is $\pi_1(w) = a_2 w_1^2 + a_6 w_1 w_2 + a_9 w_3 w_1 + a_{15} w_3 w_2 + a_{18} w_3^2$, where

$$\begin{aligned} a_2 &= \frac{1}{RE}, \qquad a_6 = -\frac{\alpha C}{E}, \\ a_9 &= \frac{2}{RE}, \qquad a_{15} = -\frac{\alpha C}{E}, \qquad a_{18} = \frac{1}{RE}. \end{aligned} \tag{A.4}$$

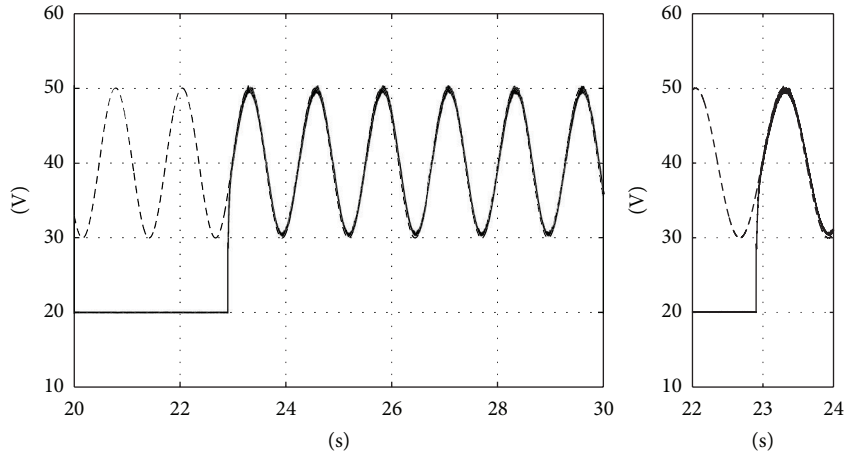

Figure 18: Output tracking of the voltage capacitor with $\alpha = 5$ rad/s, reference signal (dashed line), real-time signal (solid line).

Then, the sliding function and control are chosen of the following form:

$$s = z_2 + c_1 z_1, \qquad v = \frac{1}{2} - \frac{1}{2}\,\mathrm{sign}\,(s)\,. \tag{A.5}$$

The sampling of the former continuous-time controller by means of the explicit Euler method results as follows:

$$s_k = z_{2,k} + c_1 z_{1,k}, \qquad v_k = \frac{1}{2} - \frac{1}{2}\,\mathrm{sign}\,(s_k)\,. \tag{A.6}$$

The discrete-time steady state errors are as follows: $z_k = x_k - \pi_k(w_k) = (z_{1,k}, z_{2,k})^T$ where $x_k = (x_{1,k}, x_{2,k})^T$ and $\pi_k(w_k) = (\pi_{1,k}(w_k), \pi_{2,k}(w_k))^T$, with $\pi_{1,k}(w_k) = a_2 w_{1,k}^2 + a_6 w_{1,k} w_{2,k} + a_9 w_{3,k} w_{1,k} + a_{15} w_{3,k} w_{2,k} + a_{18} w_{3,k}^2$, $\pi_{2,k}(w) = w_{1,k} + w_{3,k}$. Finally, the exosystem is approximated to the following form:

$$\begin{aligned} w_{1,k+1} &= w_{1,k} - \alpha h w_{2,k}, \\ w_{2,k+1} &= w_{2,k} + \alpha h w_1, \\ w_{3,k+1} &= w_{3,k}. \end{aligned} \tag{A.7}$$

References

[1] U. Ribes-Mallada, R. Leyva, and P. Garcés, "Optimization of DC-DC converters via geometric programming," *Mathematical Problems in Engineering*, vol. 2011, Article ID 458083, 19 pages, 2011.

[2] J. A. Taborda, D. Burbano, and F. Angulo, "Quantization effects on period doubling route to chaos in a ZAD-controlled buck converter," *Mathematical Problems in Engineering*, vol. 2012, Article ID 526394, 19 pages, 2012.

[3] F. Esposito, G. Gentile, V. Isastia, and S. Meo, "A new bidirectional soft-switching multi-input DC-DC converter for automotive applications," *International Review of Electrical Engineering*, vol. 5, no. 4, pp. 1336–1346, 2010.

[4] J. Ciezki and R. Ashton, "The design of stabilizing controls for shipboard dc-to-dc buck choppers using feedback linearization techniques," in *Proceedings of the 29th Annual IEEE Power Electronics Specialists Conference (PESC'98)*, Fukuoka, Japan, May 1998.

[5] J. Kassakian, M. Schlecht, and G. Verghese, *Principles of Power Electronics*, Addison-Wesley, New York, NY, USA, 1991.

[6] H. Sira-Ramírez, "DC-to-AC power conversion on a "boost" converter," *International Journal of Robust and Nonlinear Control*, vol. 11, no. 6, pp. 589–600, 2001.

[7] H. Sira-Ramirez, R. Marquez-Contreras, and M. Fliess, "Sliding mode control of DC-to-DC power converters using integral reconstructors," *International Journal of Robust and Nonlinear Control*, vol. 12, no. 13, pp. 1173–1186, 2002.

[8] J. Jang, S. Choi, B. Choi, and S. Hong, "Average current mode control to improve current distributions in multi-module esonant dc-to-dc converters," in *Proceedings of the 8th IEEE International Conference on Power Electronics and ECCE Asia (ICPE & ECCE)*, Jeju, Republic of Korea, May-June 2011.

[9] J. N. Marie-Francoise, H. Gualous, and A. Berthon, "DC to DC converter with neural network control for on-board electrical energy management," in *Proceedings of the 4th International Power Electronics and Motion Control Conference (IPEMC'04)*, pp. 521–525, Xi'an, China, August 2004.

[10] D. Saifia, M. Chadli, S. Labiod, and H. R. Karimi, "H_∞ fuzzy control of DC-DC converters with input constraint," *Mathematical Problems in Engineering*, vol. 2012, Article ID 973082, 18 pages, 2012.

[11] J. L. Flores, J. L. B. Avalos, and C. A. B. Espinosa, "Passivity-based controller and online algebraic estimation of the load parameter of the DC-to-DC power converter Ćuk type," *IEEE Latin America Transactions*, vol. 9, no. 1, pp. 784–791, 2011.

[12] K. J. Astrm and B. Wittenmark, *Computer-Controlled Systems*, Prentice Hall, New York, NY, USA, 1990.

[13] S. Monaco and D. Normand-Cyrot, "Issues on nonlinear digital control," *European Journal of Control*, vol. 7, no. 2-3, pp. 160–178, 2001.

[14] N. Kazantzis and C. Kravaris, "System-theoretic properties of sampled-data representations of nonlinear systems obtained via Taylor methods," in *Proceedings of the American Control Conference*, pp. 1354–1360, Baltimore, Md, USA, July 1994.

[15] A. Stern and M. Desbrun, "Discrete geometric mechanics for variational integrators," in *Proceedings of the 33rd International Conference and Exhibition on Computer Graphics and Interactive Techniques*, Boston, Mass, USA, July-August 2006.

[16] J. Rivera, L. García, S. Ortega, and J. Raygoza, "Discrete-time modeling and control of an under-actuated robotic system," in

Proceedings of the Electronics, Robotics and Automotive Mechanics Conference (CERMA'10), pp. 508–514, Morelos, Mexico, October 2010.

[17] A. Navarrete, J. Rivera, J. J. Raygoza, and S. Ortega, "Discrete-time modeling and control of PMSM," in *Proceedings of the Electronics, Robotics and Automotive Mechanics Conference (CERMA'11)*, pp. 258–263, Morelos, Mexico, November 2011.

[18] V. I. Utkin and H. C. Chang, "Sliding mode control on electromechanical systems," *Mathematical Problems in Engineering*, vol. 8, no. 4-5, pp. 451–473, 2002.

[19] V. Utkin, J. Guldner, and J. Shi, *Sliding Mode Control in Electromechanical Systems*, CRC Press, New York, NY, USA, 1999.

[20] J. Rivera, L. Garcia, C. Mora, J. J. Raygoza, and S. Ortega, "Super-twisting sliding mode in motion control systems," in *Sliding Mode Control*, A. Bartoszewicz, Ed., pp. 237–254, InTech, Rijeka, Croatia, 2011.

[21] Yu. B. Suris, "Hamiltonian methods of Runge-Kutta type and their variational interpretation," *Matematicheskoe Modelirovanie*, vol. 2, no. 4, pp. 78–87, 1990.

[22] J. Moser and A. P. Veselov, "Discrete versions of some classical integrable systems and factorization of matrix polynomials," *Communications in Mathematical Physics*, vol. 139, no. 2, pp. 217–243, 1991.

[23] J. E. Marsden and M. West, "Discrete mechanics and variational integrators," *Acta Numerica*, vol. 10, pp. 357–514, 2001.

[24] M. West, *Variational integrators [Ph.D. thesis]*, Division of Engineering and Applied Science, California Institute of Technology, Pasadena, Calif, USA, 2004.

[25] R. Ortega, A. Lora, P. J. Nicklasson, and H. Sira-Ramrez, *Passivity-Based Control of Euler-Lagrange Systems: Mechanical, Electrical, and Electromechanical Applications*, Springer, New York, NY, USA, 1998.

[26] B. Castillo-Toledo, S. Di Gennaro, A. G. Loukianov, and J. Rivera, "Hybrid control of induction motors via sampled closed representations," *IEEE Transactions on Industrial Electronics*, vol. 55, no. 10, pp. 3758–3771, 2008.

[27] J. Rivera, A. G. Loukianov, and B. Castillo-Toledo, "Discontinuous output regulation of the Pendubot," in *Proceedings of the 17th World Congress, International Federation of Automatic Control (IFAC'08)*, Seoul, Republic of Korea, July 2008.

[28] A. Loukianov, J. Rivera, F. Chavira, and S. Ortega, "Discontinuous output regulation for a DC-to-AC boost converter," in *Proceedings of the 9th International Conference on Electrical Engineering, Computing Science and Automatic Control*, Mexico City, Mexico, September 2012.

[29] X. Yu and O. Kaynak, "Sliding-mode control with soft computing: a survey," *IEEE Transactions on Industrial Electronics*, vol. 56, no. 9, pp. 3275–3285, 2009.